Experimental Progress Towards Testing the Behavior of Gravity at the 20-micron Distance Scale

By M.P. Ross[A], J.S. Johnson[A], I.S. Guerrero[A] , H.F. Leopardi[B], and C.D. Hoyle[A]

[A]Department of Physics and Astronomy, Humboldt State University, Arcata, CA; [B]NIST/University of Colorado, Boulder, CO

Abstract

Due to discrepancies between the Standard Model and General Relativity, questions have arisen about the fundamental behavior of gravity. Many theories have speculated that gravity behaves fundamentally different at short ranges with respect to the predictions of Newtonian theory. These discrepancies have led the Humboldt State Gravitational Research Lab to begin constructing an experiment that will test the behavior of gravity at distances that have yet to be explored. The experiment has been improved upon in many aspects and has entered an initial data acquisition phase.

1. Introduction

1.1 Motivation

The behavior of gravity at short ranges has been called into question by many modern theories. Some speculate that there are extra dimensions with sizes from 100 m to 1 mm which Standard Model particles cannot access, yet gravity can [1]. This would cause gravity to change behavior at distance scales similar to the dimension's size. Also, many variations of string theory call for changes to the behavior of gravity [2, 3]. Short range tests of gravity are one of the few ways in which these predictions can be probed. For a more detailed review, see Reference [4].

1.2 Inverse Square Law Tests

The Inverse-Square Law (ISL) of gravity is a fundamental part of Newtonian gravity and states that the force of gravity is proportional to the inverse-square of distance, $F_g \propto 1/r^2$. Since Newtonian gravity is an approximation for General Relativity in the weak-field limit, tests of the ISL are fundamentally tests of General Relativity. Deviations of the ISL are traditionally parameterized by assuming an additional Yukawa interaction, which gives a potential energy between two point masses as:

$$V(r) = -\frac{Gm_1m_2}{r}(1+\alpha e^{-r/\lambda}), \quad (1)$$

where α is the strength of the deviation and λ is the length scale at which the deviations become relevant. This potential energy can describe many of the possible theoretical situations and simplifies to the Newtonian potential if r >> λ or α = 0. Many ISL test have been conducted which set limits in the α - λ parameter space, as shown in Figure 1. Also shown are two projected sensitivity curves for the Humboldt experiment, described below, which correspond to analyzing only the first or second harmonic of the gravitational signal.

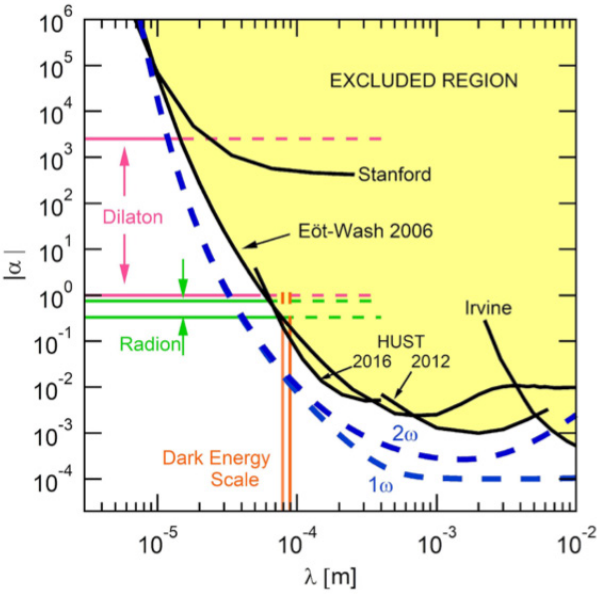

Figure 1: α - λ parameter space for ISL deviations. Black curves correspond to previous experiments' limits [5,6] while the blue dashed curves correspond to the projected sensitivity of the Humboldt experiment [7]. The yellow region is the region where there are no deviations from the ISL within 95% confidence. The dilaton, radion, and dark energy scale regions correspond to various theoretical situations that call for certain parameter ranges, as described in Reference [8].

1.3 Weak Equivalence Principle Tests

The weak equivalence principle (WEP) can be stated as "the gravitational force felt by an object is independent of its composition." The WEP is a central tenet of General Relativity. WEP violations can be parameterized by assuming a fifth force of nature that is related to some linear combination of the baryon and lepton numbers. This fifth force would couple to a "charge", $\tilde{q}$, that can be parameterized by:

$$\tilde{q} = \tilde{g}[Z\cos(\tilde{\psi}) + N\sin(\tilde{\psi})], \quad (2)$$

where Z and N are the atomic number and neutron number, respectively, of the material in question and $\tilde{g}$ is a coupling constant. Note that this is easily transformed through the mixing angle, $\tilde{\psi}$, to the baryon number, B, and the lepton number, L, for an electrically neutral material by using the relations B=Z+N and L=Z. This coupling leads to a potential energy between two point masses of the form:

$$V(r) = -\frac{Gm_1m_2}{r}\left(1+\tilde{\alpha}\left[\frac{\tilde{q}}{\tilde{g}\mu}\right]_1\left[\frac{\tilde{q}}{\tilde{g}\mu}\right]_2 e^{-r/\lambda}\right), \quad (3)$$

where μ is the mass in atomic mass units (u), $\tilde{q}$ is the fifth force "charge" as described above, $\tilde{g}$ is a coupling constant, λ is the Compton wavelength of the fifth force exchange boson, and $\tilde{\alpha} = \pm\tilde{g}^2/(4\pi Gu^2)$ (+ and - for scalar and vector coupling, respectively). The quantities inside the brackets are of object 1 and 2 as labeled. These parameters have had limits set on them by previous experiments, which are shown in Figure 2.

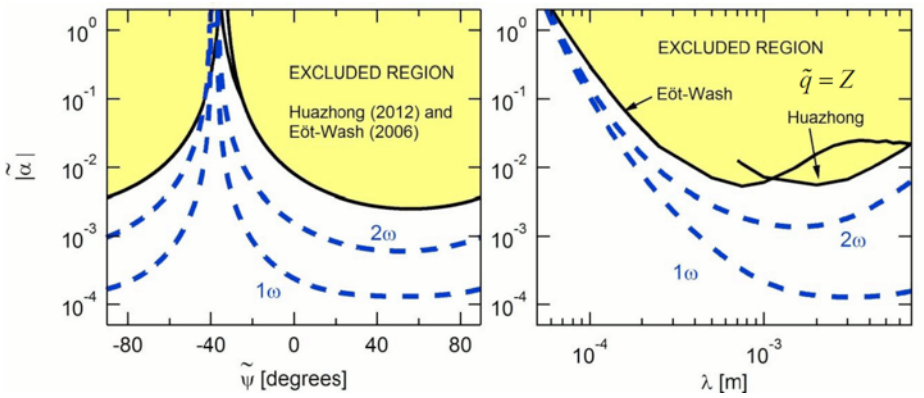

Figure 2: On the left is the $\tilde{\alpha}$ - $\tilde{\psi}$ parameter space, with $\lambda = 1$ mm, and on the right is the $\tilde{\alpha}$ - λ parameter space, with $\tilde{q} = Z$, for the above WEP deviation potential. Black curves correspond to previous experiments' limits while the blue dashed curves correspond to the projected sensitives of the Humboldt experiment. [7]. The yellow region is the region where there are no deviations from the WEP within 95% confidence.

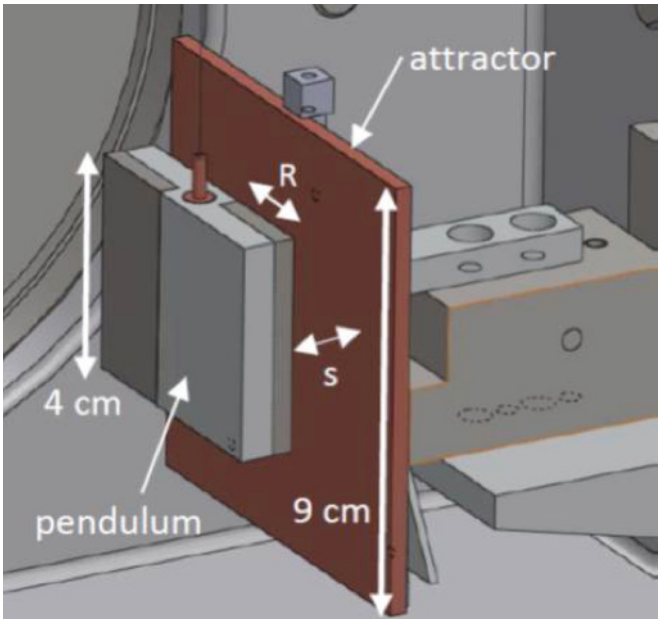

Figure 3: Pendulum-Attractor Geometry. The copper plate is the attractor mass held rigidly to the stage of a stepper motor. This facilitates the oscillatory motion. Just in front of the attractor is the suspended pendulum. The lighter gray section is aluminum while the dark gray is titanium. Not shown is a 25μm thick BeCu electrostatic shield which will be stretched in between the attractor and the pendulum.

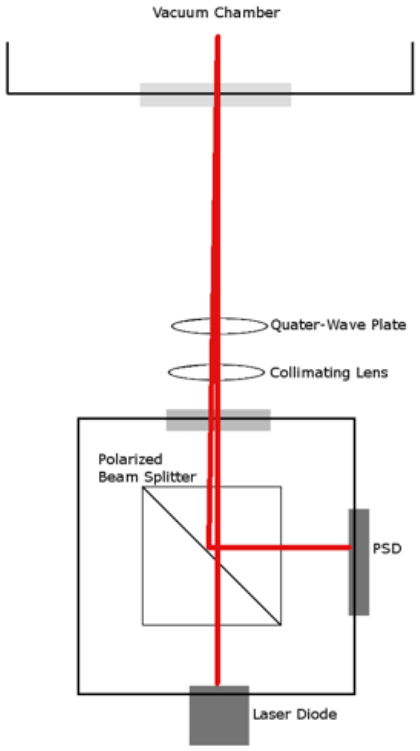

Figure 4: Autocollimator Schematic. This system was built and tested on a benchtop optical table before installation [9]. Noise tests of the system found the noise floor at 0.01 Hz, the frequency of interest in the Humboldt experiment, to be about 1.0 x 10^{-7} $rad/\sqrt{Hz}$ which corresponds to a nanoradian sensitivity in about 4 hours [9]. This performance exceeded the requirements and the system was subsequently implemented onto the apparatus.

2. Experiment Overview

At Humboldt State, an experiment is being constructed that will probe the WEP and ISL at untested length scales for a given deviation strength. The experiment consists of a rectangular torsion pendulum in close proximity to a rectangular plate attractor mass, shown in Figure 3. This copper attractor mass is modulated toward and away from the pendulum, thus inducing a time-varying torque on the pendulum. The motion of the pendulum is recorded using an optical system described in Section 2.1. The pendulum consists of an aluminum step with two titanium blocks attached to each side, making a complete rectangular prism. The pendulum is hung using a 25μm diameter tungsten fiber. Due to the use of two different materials, the atomic number and neutron number of either side differs on the surface that faces the attractor. This design allows for tests of the WEP as described in Section 1.3.

2.1 Optical Measurement System

To meet expected sensitivities, an optical system able to measure angles to one nanoradian uncertainty per day is required. The angular uncertainty at a given frequency can be determined by:

$$\Delta\theta = \frac{A}{\sqrt{t}} \qquad (4)$$

where A is the noise floor at that frequency and t is the amount of time the angle is recorded. To achieve nanoradian uncertainty for a one-day data run, the noise floor would have to be less than 3x10^{-7} $rad/\sqrt{Hz}$ at the frequency of interest [9]. An autocollimator was designed and implemented with this goal in mind. It consists of a polarized laser beam directed through a polarized beam splitter, collimating lens, and a quarter wave plate before striking the pendulum and returning through a similar path. A schematic of the autocollimator is shown in Figure 4. The use of a polarizing beam splitter and a quarter-wave plate allow the system to distinguish between outgoing and incoming beams. The outgoing beam is originally linearly polarized such that it is transmitted through the beam-splitter. It is then circularly polarized at the quarter-wave plate, switches orientation when reflected off the pendulum, and then is linearly polarized when it returns to the quarter-wave plate. Due to the switched circularly polarized orientation, the returning beam is polarized perpendicularly to the

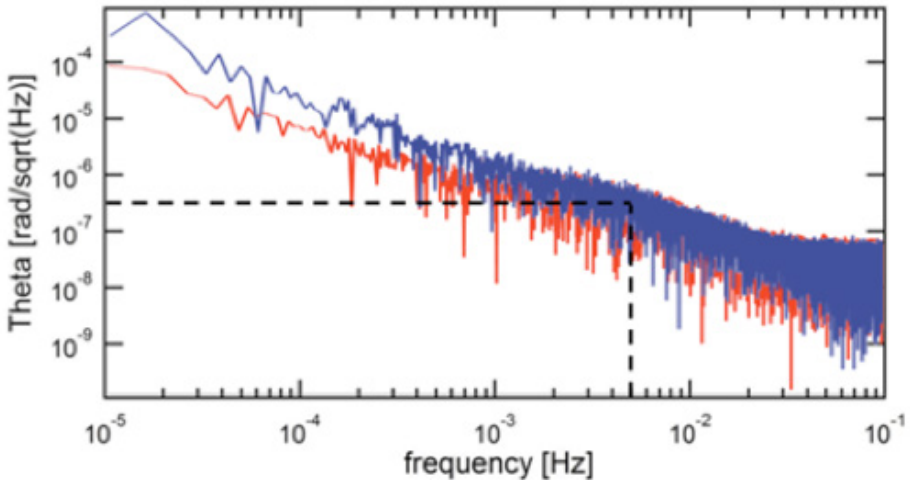

Figure 5: Autocollimator Benchtop Noise Tests. The red data is a noise run with the laser off while the blue is with the laser on. The black dashed line corresponds to the sensitivity requirements of the system. Figure taken from Reference [9].

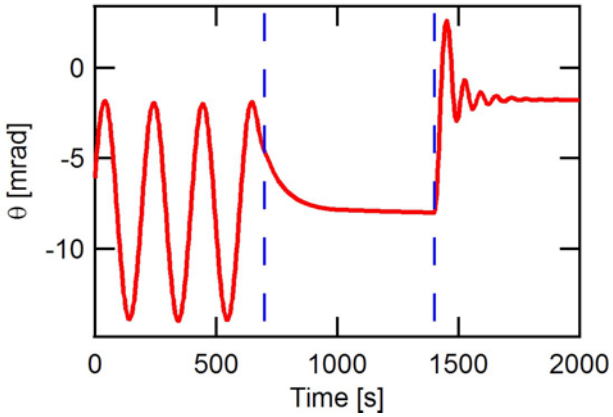

Figure 6: A demonstration of pendulum controls. At the time of the first dashed line, the electrode controls were turned on which subsequently damped out any motion of the pendulum. At the time of the second dashed line, the equilibrium position of the pendulum was shifted and the electrode system damped out the resultant motion.

outgoing beam causing it to reflect off of the beam-splitter and to a position sensitive device (PSD). The PSD outputs voltages for each of the four sides which correspond to the beam's position. These voltages are sent through an amplification circuit which outputs three signals: the difference between the two horizontal sides, the difference between the two vertical sides, and the sum of the two horizontal sides. These are then recorded using a LabVIEW data acquisition program. The ratio of the difference and the sum of the horizontal sides is proportional to the angle of the pendulum, allowing one to measure the angle of the pendulum over time.

2.2 Pendulum Control Systems

Due to the close proximity required for this experiment, the pendulum's free resonant motion and position must be well controlled prior to taking data.

2.2.1 Pendulum Positioning Assembly

To be able to make the measurements required for this experiment, the ability to translate the pendulum about the chamber and rotate the pendulum about its vertical axis is necessary. This is achieved using a translation stage which allows for three directional translations of the pendulum's connection point and a rotation stage which allows for rotations about the vertical axis. These controls allow the pendulum to be moved close to the attractor mass, aim the reflected beam back to the autocollimator, and manually damp unwanted motion of the pendulum.

2.2.2 Eddy Current Damper

The Humboldt experiment is only interested in the torsional motion of the pendulum, however, there are many other modes of motion that can influence the measurements. These include swing in both horizontal directions. To mitigate these effects, an eddy current damper was installed which consists of a pre-hanger fiber connected to an aluminum disk from which the pendulum is hung. The aluminum disk is suspended between the north and south poles of two separated ring magnets. This adds damping for any motion that is not uniform about the axis of the fiber due to the eddy currents caused by the change of magnetic flux through the aluminum disk.

2.2.3 Electrode Control

The thinness of the fiber causes the pendulum to react drastically to any shock or twist that may happen while work is done on or around the chamber. The pendulum will have a large quality factor due to various environmental controls, described in Section 2.3.1. Because of this, an electrode control system was developed which applies damping torques to the pendulum in order to decrease the amplitude before taking data. The system consists of two rectangular electrodes positioned in close proximity to the pendulum on the opposite side from the attractor mass. Voltages are applied based on PID feedback from the autocollimator's angular signal. The PID loop is controlled using a LabVIEW program allowing for manual changing of the PID parameters.

2.3 Environmental Effects

The sensitivity of these tests requires a very low noise apparatus. Thus, many efforts to decrease environmental noise sources have been or will be implemented.

2.3.1 Vacuum System

The pendulum and attractor mass are both placed inside a rectangular freestanding vacuum chamber. This is pumped down to ~10^{-6} Torr via a turbo pump, which stops any convection currents inside the chamber and decreases the heat conduction pathways from the walls of the chamber to the pendulum. Being at ultra-high vacuum also decreases gas damping of the pendulum thus increasing the pendulum's quality factor to approximately 3500.

2.3.2 Electrostatic Shielding

The pendulum is gold-coated and the pendulum-fiber assembly is surrounded by electrostatic shielding, which decreases both electrostatic coupling and patch charge build up. Any electrostatic coupling would overpower gravitational signals due to the dramatic difference in strength between the two forces.

2.3.3 Thermal Controls

Due to the thinness of the tungsten fiber, any temperature fluctuations of the fiber will produce a torque on the pendulum. To decrease these effects, many steps have been taken to stabilize the temperature of the fiber. The shielding that surrounds the fiber has a large mass, thus decreasing any high frequency coupling to temperature fluctuations of the walls. The entire chamber is placed inside a large thermal isolation box which has its temperature controlled to within 10 mK, thus decreasing low-frequency temperature fluctuations. Multiple temperature sensors are placed throughout

the room and within the chamber to monitor the temperature while the experiment is running [10].

2.3.4 Magnetic Measurements

The ambient magnetic field in the experiment is not well controlled. To account for this, the magnetic moment of the pendulum in the horizontal plane was measured by applying a time varying magnetic field to the chamber and measuring the pendulum's response. Using this, the torque that would be caused by a normal varying of the earth's magnetic field was calculated and found this to be below the autocollimator's noise limit [10].

2.3.5 Tilt Compensation System

Although the pendulum always hangs along the local vertical axis, the chamber, and thus the optical systems, can tilt along both horizontal directions. Such a tilt would be indistinguishable from tilt of the pendulum. To account for this, there are tilt sensors, one for each direction, placed on top of the chamber. A feedback system which extends the legs of the chamber by thermal expansion to decrease tilt is currently being developed.

In order to compensate for this, and any other tilt the apparatus may experience, a system is being designed which will read tilt information from tilt sensors placed on top of the apparatus and applies heat to the three legs of the apparatus to compensate for this tilt. Figure 7 shows the tilts that the apparatus experiences over the course of 4.5 days with the tilt compensation system turned on and off. The system currently decreases the tilts by roughly a factor of two, which was found to be an acceptable level of compensation, and will be improved upon in future work.

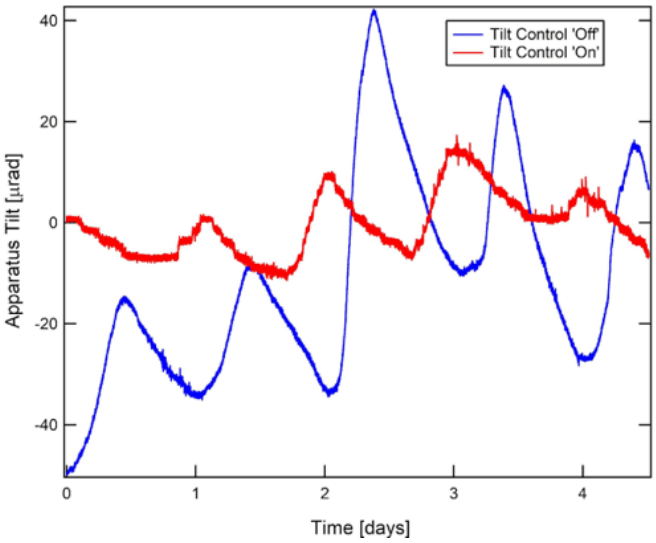

Figure 7: Time series of measured chamber tilt with tilt compensation system turned on (red) and off (blue). The tilt control system decreases apparatus tilts by roughly a factor of two.

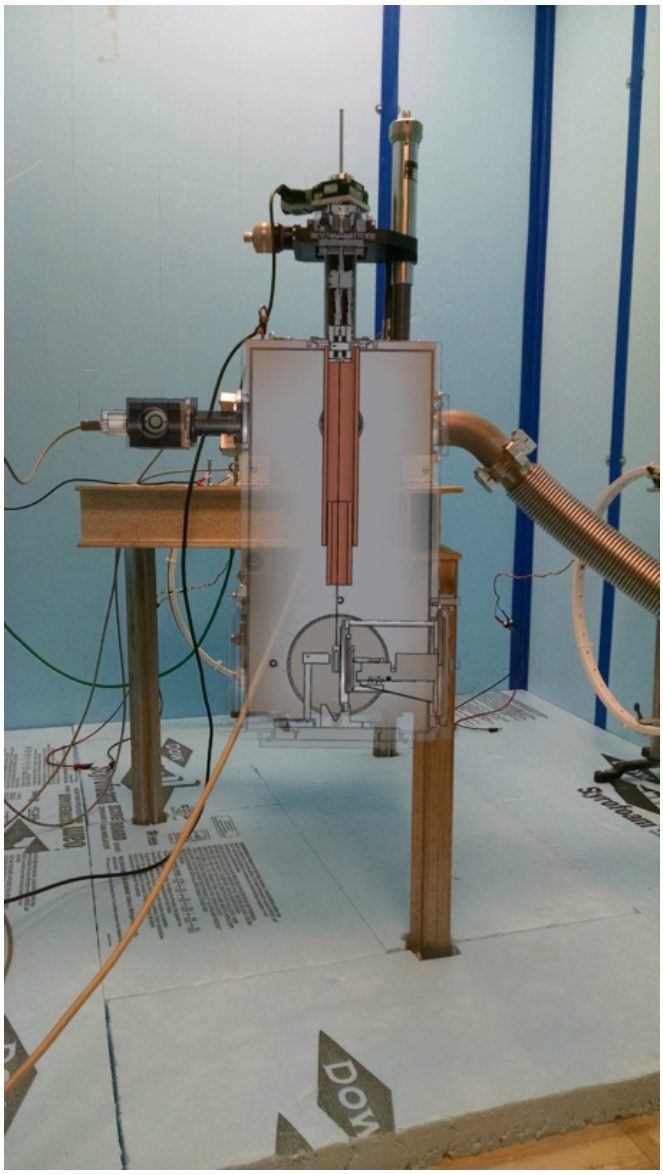

Figure 8: A cross section of the designs for the apparatus overlaid onto a picture of the vacuum chamber. The black box on the left of the chamber is the autocollimator. On the top is the pendulum positioning assembly and eddy current damper. At the bottom of the chamber is the electrode control system, pendulum, and attractor mass assembly.

3. Signal Processing and Data Analysis

Data recorded by the acquisition program is analyzed using a custom python script. Recent upgrades to the analysis software have placed the experiment in a position where preliminary data can be fully analyzed.

3.1 Converting the autocollimator output to a twist angle

The PSD output voltages are used to determine the pendulum's twist by

$$\theta = c_1\left(\frac{\Delta_s}{\Sigma}\right) + c_2\left(\frac{\Delta_s}{\Sigma}\right)^2, \quad (5)$$

where Δ_s is the voltage proportional to the difference between the two horizontal sides and Σ is the voltage proportional to the sum of the two horizontal sides of the PSD. The linear and quadratic calibration coefficients c_1 and c_2 can be determined by remotely adjusting the rotation stage by a known angle and comparing the new equilibrium to the autocollimator output. We found

$$c_1 = 1.0351^\circ \pm 0.00505^\circ.$$

Data was recently taken to determine c_2. However, this data was shown to be inconsistent. Unfortunately, the apparatus was taken out of vacuum before additional tests were done. Furthermore, upon opening the apparatus, it was found that the pendulum had a slight but noticeable tilt so that it did not hang perpendicular to the incident beam. In response, work is being done to distinguish potential problems that might impede future determination of the coefficient.

3.2 Filtering out the free oscillations

Because the pendulum's free oscillation provides no information about the ISL or WEP, a digital filter is utilized to suppress this signal before analyzing the attractor effects. This "torsion filter" assigns a new value

$$\theta_f(t) = \frac{1}{2}\left[\theta\left(t-\frac{\tau_0}{4}\right)+\theta\left(t+\frac{\tau_0}{4}\right)\right]A_f, \quad (6)$$

to a data point by averaging two data points a quarter of a torsion period on either side, where τ_0 is the period of the pendulum's free oscillation (about 350 seconds) and θ is the interpolated value of the twist.

The digital filter described inherently affects the attractor signal in addition to the pendulum's free oscillation. To account for this, the term below is applied

$$A_f = sec\left(\frac{\pi\omega}{2\Omega}\right), \quad (7)$$

where ω is the attractor mass frequency and $\Omega = \frac{2\pi}{\tau_0}$, that restores the signal of interest. An example of the effectiveness of the filter is shown in Figure 10.

3.3 Analysis of the twist data

The data is subdivided into many "cuts" containing an arbitrary integer number of oscillations of the attractor mass. It was found that fourteen oscillations (about 2800 seconds) worked well for preliminary data runs. For each cut, θ_f is fitted as a function of time with

$$\theta_{th}(t) = \sum_n [b_n sin(n\omega t) + c_n cos(n\omega t)] + \alpha + \beta t, \quad (8)$$

where the sum accounts for multiple harmonics and α and β account for fiber drift. A "chi-squared" statistic can be computed

$$\tilde{\chi}^2 = \sum_{i=1}^{N_d} (\theta_f(t_i) - \theta_{th}(t_i))^2, \quad (9)$$

where N_d is the number of points contained in a cut, that reflects the goodness of the fit. Based on the $\tilde{\chi}^2$ distribution, as shown in Figure 11, and other criterion, one can reject specific cuts that are dominated by environmental disturbances before inferring the torque applied on the pendulum.

For all N_c cuts that survive the rejection criterion, the mean and standard deviation of the b_n coefficients can be calculated as

$$\overline{b_n} = \frac{1}{N_c}\sum_{i=1}^{N_c} b_n(i); \sigma_{\overline{b_n}} = \sqrt{\frac{1}{N_c(N_c-1)}\sum_{i=1}^{N_c}(b_n(i)-\overline{b_n})^2}, \quad (10)$$

with similar equations applying to the c_n coefficients. The applied torque on the pendulum, N, can then be found with

$$N = \kappa\theta f_i, \quad (11)$$

where κ is the torsional spring constant of the fiber and $f_i = A_i e^{i\Phi_i}$, which accounts for the effects of pendulum inertia, where

$$A_i = \sqrt{[1-(\omega/\Omega)^2]^2 + (1/Q)^2};$$
$$\Phi_i = tan^{-1}\frac{\Omega^2}{Q(\Omega^2-\omega^2)}, \quad (12)$$

and Q is the quality factor of the torsion oscillator [5].

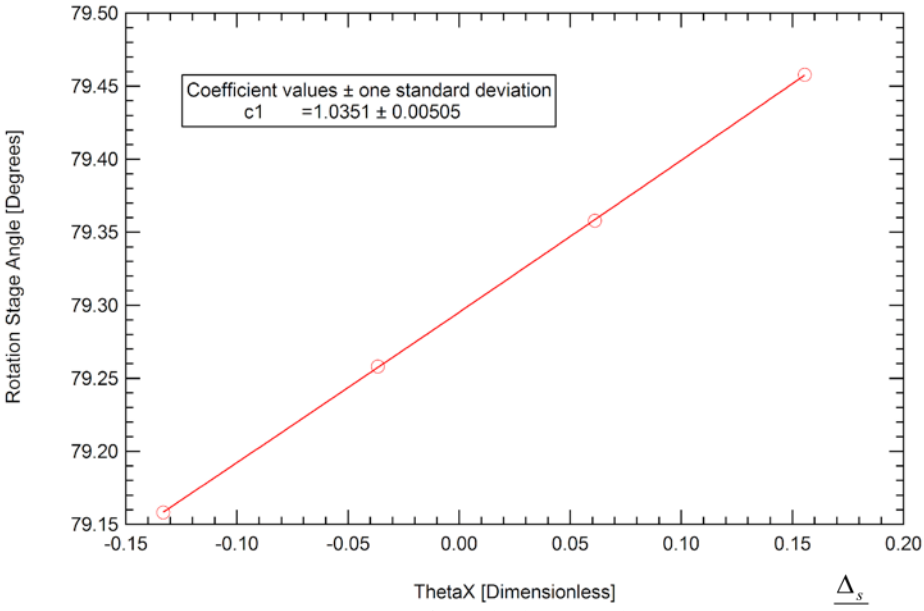

Figure 9: Determination of c_1. The horizontal axis is the quantity $\frac{\Delta_s}{\Sigma}$.

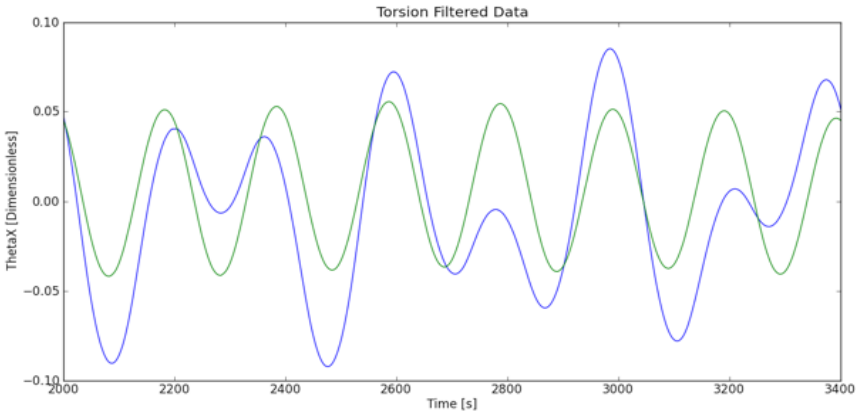

Figure 10: Torsion filtered data. The blue curve corresponds to raw data, while the green curve is data with the pendulum's free oscillation filtered out. The vertical axis is the quantity $\frac{\Delta_s}{\Sigma}$ described in section 3.1.

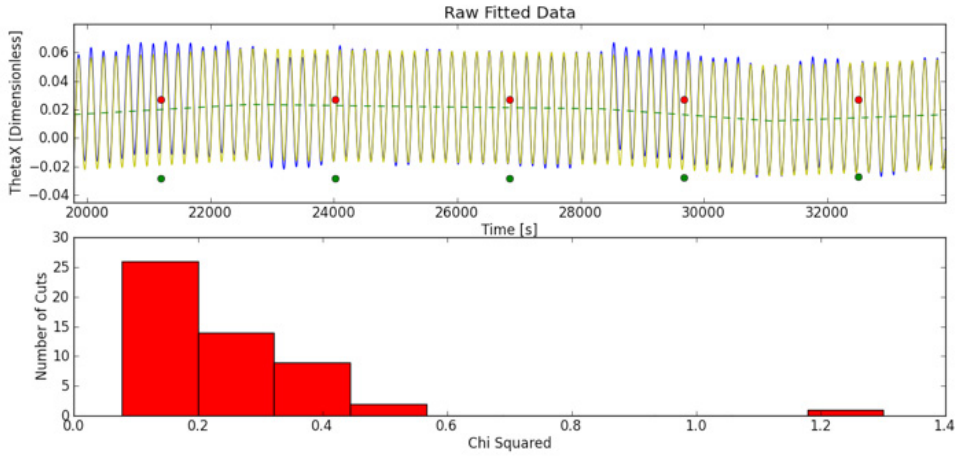

Figure 11: Fitted data for the 1ω signal. Top plot: 5 cuts of length 2826 seconds. The blue curve corresponds to θ_f, while the yellow curve is θ_{th}. The green and red circles are the b_n and c_n coefficients respectively. The green dashed line corresponds to the polynomial $\alpha + \beta t$. Bottom plot: a typical "chi squared" distribution. For this distribution, the cut whose $\tilde{\chi}^2$ is above the 1.0 bin would most likely be rejected based upon correlation with an environmental disturbance identified with other sensors; all other cuts are reasonable since they have $\tilde{\chi}^2$ of order less than 1.

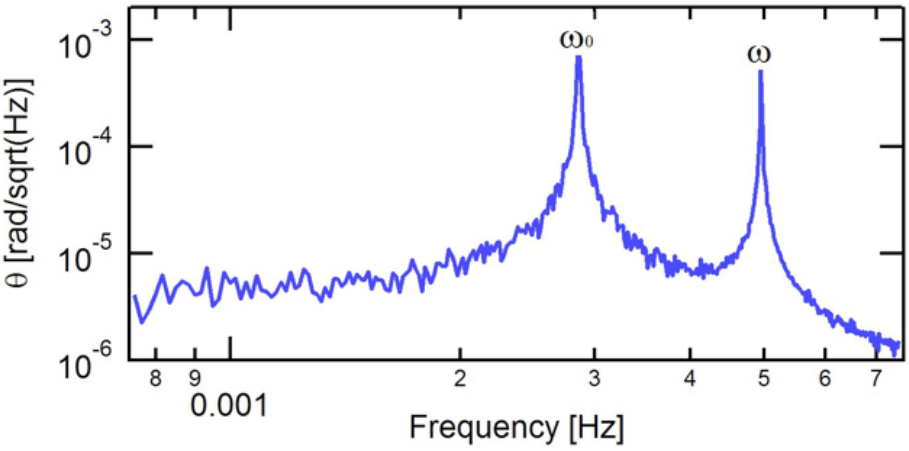

Figure 12: A section of the amplitude spectral density of the pendulum's motion. ω_0 is the natural frequency of the pendulum and ω is the frequency of oscillation of the attractor mass.

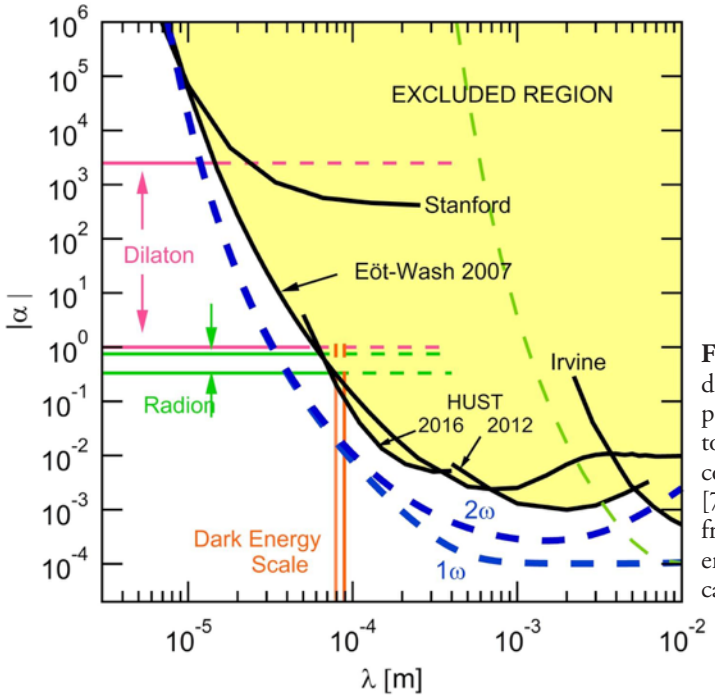

Figure 13: α - λ parameter space for ISL deviations. The green dash curve is preliminary limits from recent runs with minimum pendulum-attractor separation of 8 mm. Black curves correspond to previous experiments' limits [5,6] while the blue dashed curves correspond to the projected sensitivity of the Humboldt experiment [7]. The yellow region is the region where there are no deviations from the ISL within 95% confidence. The dilaton, radion, and dark energy scale regions correspond to various theoretical situations that call for certain parameter ranges, as described in Reference [8]

4. Preliminary Data

Recent updates, as discussed above, have brought the experiment to a point where the data may contain gravitational information. Data has recently been taken which appears to be of improved quality over other runs. This data has not yet been analyzed to the point where one could say if there is any gravitational information, but the current phase of analysis is relevant nonetheless.

4.1 Attractor mass run

Data taken in 2015 includes an attractor mass run in which the attractor mass was driven at a frequency of 5 mHz and with an amplitude of 1 mm. Figure 12 is a section of the amplitude spectral density of this attractor mass run. In this figure, ω_0 is the frequency of the natural oscillation of the pendulum, while ω is the frequency of the attractor mass oscillation. This data clearly indicates some interaction between the attractor mass and pendulum, however, whether this is due to gravity or other forces has yet to be determined.

The above spectrum exhibits the ability to operate a torsion balance while modulating the attractor mass without broadband noise injection. With future systematic studies and improvements, non-gravitational coupling paths between the attractor and pendulum can be rejected while also decreasing the noise and environmental effects.

4.2 Preliminary Limits

With the ability to resolve interactions between the attractor and pendulum, preliminary limits can be set on ISL violations which are shown in Figure 13. These limits were obtained using data with pendulum-to-attractor separation of 8 mm and are only an estimate due to unconstrained systematics that are currently being investigated. With improved systemic understanding and smaller pendulum-attractor separations, the limits are expected to reach to lower λ scales and approach the experiment's design sensitivity.

Conclusion

At Humboldt State, an apparatus has been constructed that can controllably measure the interactions between a torsion pendulum and an attractor mass. This apparatus has the promise to test both the Inverse-Square Law and the Weak Equivalence Principle at unprecedented length scales and has begun to set preliminary limits on Inverse Square Law violations. With continued systematic understanding and experimental control, these limits are expected to approach the experiments design sensitivity which will increase the understanding of gravitational interactions in novel regimes.

Acknowledgements

We are thankful for financial support from the National Science Foundation (Grants PHY-1065697, PHY-1306783, and PHY-1606988), Research Corporation (Cottrell College Science Award CC6839), and the Humboldt State University College of Natural Resources and Sciences (CNRS), Office of Research and Graduate Studies, and President's Office. Special thanks to Dr. C.D. Hoyle for the mentoring and guidance.

References

1 S. Dimopoulos, N. Arkani-Hamed, and G.R. Dvali. "The hierarchy problem and new dimensions at a millimeter." Phys. Lett. B, 429:263–272, 1998.

2 S. Dimopoulos, N. Arkani-Hamed, and G.R. Dvali. "New dimensions at a millimeter to a fermi and superstrings at a tev." Phys. Lett. B, 436:257, 1998.

3 M. Kolanovic, G. Dvali, G. Gabadadze, and F. Nitti. "Scales of gravity." Phys. Rev. D, 65:024031, 2001.

4 Jiro Murata and Saki Tanaka, "A review of short-range gravity experiments in the LHC era," Class. Quantum Grav. 32 033001, 2015.

5 C. D. Hoyle, D. J. Kapner, B. R. Heckel, E. G. Adelberger, J. H. Gundlach, U. Schmidt, and H. E. Swanson. "Submillimeter tests of the gravitational inverse-square law." Phys. Rev. D, 70:042004, Aug 2004.

6 Wen-Hai Tan, Shan-Qing Yang, Cheng-Gang Shao, Jia Li, An-Bin Du, Bi-Fu Zhan, Qing-Lan Wang, Peng-Shun Luo, Liang-Cheng Tu, and Jun Luo. "New Test of the Gravitational Inverse-Square Law at the Submillimeter Range with Dual Modulation and Compensation." Phys. Rev. Lett. 116, 131101, 2016.

7 David W. Shook. "Experimental tests of gravity below the 50-micron distance scale." Proceedings of The National Conference On Undergraduate Research (NCUR), 2010.

8 Holly Leopardi, and David Smith. "Short-range tests of gravitational physics." Proceedings of The National Conference On Undergraduate Research (NCUR), pages 178–186, 2013.

9 Holly Leopardi. "Tests of gravity below fifty microns." Proceedings of The National Conference On Undergraduate Research (NCUR), pages 357–162, 2012.

10 Andrew C. Harter. Crystal Cardenas, and Michael P. Ross. "Experimental progress on tests of gravity at 20 microns." Proceedings of The National Conference On Undergraduate Research (NCUR), pages 811–819, 2014.